3D defect detection of connectors based on structured light*

JI Yue (纪越)[1], **CHEN Yang** (陈扬)[1], **SONG Li-mei** (宋丽梅)[1]**, **YANG Yan-gang** (杨燕罡)[2], **and YANG Huai-dong** (杨怀栋)[3]

1. Key Laboratory of Advanced Electrical Engineering and Energy Technology, Tiangong University, Tianjin 300387, China

2. School of Mechanical Engineering, Tianjin University of Technology and Education, Tianjin 300222, China

3. Department of Precision Instrument, Tsinghua University, Beijing 100084, China

(Received 10 December 2019; Revised 19 February 2020)

In order to realize the rapid detection of three-dimensional defects of connectors, this paper proposes a method for detecting connector defects based on structured light. This method combines structured light with binocular stereo vision to obtain three-dimensional data for the connector. Point cloud registration is used to identify defects and decision trees are used to classify defects. The accuracy of the 3D reconstruction results in this paper is 0.01 mm, the registration accuracy of the point cloud reaches the sub-millimeter level, and the final defect classification accuracy is 94%. The experimental results prove the effectiveness of the proposed three-dimensional connector defect detection method in connector defect detection and classification.

Document code: A **Article ID:** 1673-1905(2021)02-0107-5

DOI https://doi.org/10.1007/s11801-021-9212-8

The defect of the connector is an important factor affecting the safety of industrial production. Common defects such as missing pin, broken pin, and curved pin would cause damage to the connector, which not only shortens the life of the part, but also poses a potential serious safety hazard to industrial generation. Therefore, the research and development of automatic detection methods for connector defects is very important. Over the past two decades, the use of two-dimensional imaging techniques to detect small defects has matured. However, there are still some problems that have not yet been resolved. Der-Baau Perng uses a Fourier transform based defect recovery technique to detect thread defects[1]. However, the defect detection that can only be implemented by this method cannot be used in complex scenes. Chung-Feng Jeffrey Kuo uses the K-means clustering method to distinguish the appearance, pad area and illuminating area of the chip[2]. The effective two-step back propagation neural network identifies the features of each part and completes the defect detection. The recognition effect depends on a large number of samples to be tested, so it is necessary to collect a large number of defect detection samples to ensure the recognition accuracy. Compared with the traditional method, the non-contact optical 3D measurement method can greatly improve the detection accuracy, and is an important key technology to improve quality and productivity[3-5]. Mei-Chin Lee proposed an application of X-ray computed tomography in nondestructive testing of 3D-IC packages[6]. However, this method is costly and insufficient in accuracy. Wei Z. uses the principle of laser interference to obtain the height of BGA packaged chips[7]. However, the laser interferometry is slow and cannot be used in real time.

This paper designs a three-dimensional detection system combining binocular camera and structured light. The traditional binocular stereo vision method has a poor reconstruction effect for scenes with less texture features. Combining binocular stereo vision and structured light, this method can add features to the reconstructed object, and effectively result in the occlusion problems in monocular vision, reduce the complexity of matching and achieve high-precision matching. Then a 3D connector defect detection method is proposed. The method first extracts the point cloud of the connector and then calculates the deviation between the defect point cloud and the standard point cloud model. Thereafter, for the defect data, the stitch is segmented using the K-means clustering algorithm and the feature for extracting each stitch data is extracted. Finally, a decision tree classifier is used to identify the type of pin defect.

* This work has been supported by the National Natural Science Foundation of China (Nos.61078041 and 51806150), the Natural Science Foundation of Tianjin (Nos.16JCYBJC15400, 15JCYBJC51700 and 18JCQNJC04400), the State Key Laboratory of Precision Measuring Technology and Instruments (Tianjin University) and the Program for Innovative Research Team in University of Tianjin (No.TD13-5036), and the Tianjin Enterprise Science and Technology Commissioner Project (No.18JCTPJC61700).

** E-mail: lilymay1976@126.com

The key technologies of 3D pin connector defect detection include the 3D data acquisition and 3D point cloud processing aspects. To obtain high-precision 3D data, this paper uses the TWPSP method[8] to get 3D data of the pin connector. The TWPSP method, three fringe patterns with proper wavelengths are projected on the object, and the wrapped phase can be obtained with the three proper wavelengths directly, i.e., the calculations of the equivalent wavelengths and their corresponding phase maps are not needed. The advantage of this method is that it is not necessary to superimpose the phases of different wavelengths to obtain an equivalent phase map of a higher wavelength, and it is possible to directly obtain the wrapped phase at three suitable wavelengths, thereby reducing the effects of noise and reducing the reconstruction time.

Assuming that modulated images acquired by the camera are denoted by I_k, the six-step phase-shift method adopted in this paper can be described by

$$I_k(x,y)=A(x,y)+B(x,y)\cos\left(\phi(x,y)+\frac{\pi\times k}{3}\right),$$
$$k=0,1...5, \tag{1}$$

where $A(x, y)$ is the background light intensity, $B(x, y)$ is the modulation light intensity, and $\phi(x, y)$ is wrapped phase.

For the existing three wavelength phase shift profilometry method, it uses wavelengths of λ_1=21 pixels, λ_2=18 pixels and λ_3=16 pixels as the modulation wavelength of the projected fringes. Based on these three basic wavelengths, longer equivalent wavelength λ_{12}=126 pixels, λ_{23}=144 pixels, λ_{123}=1 008 pixels can be calculated. Equivalent wavelengths can be calculated by

$$\lambda_{12}=\left|\frac{\lambda_1\times\lambda_2}{\lambda_1-\lambda_2}\right|,\ \lambda_{23}=\left|\frac{\lambda_2\times\lambda_3}{\lambda_2-\lambda_3}\right|,\ \lambda_{23}=\left|\frac{\lambda_{12}\times\lambda_{23}}{\lambda_{12}-\lambda_{23}}\right|. \tag{2}$$

This paper directly selects λ_1=1 008 pixels, λ_2=144 pixels and λ_3=16 pixels as the modulation wavelength of projected stripes and corresponding phase value $\phi_i(x, y)$ can be expressed by

$$\phi_i(i,j)=\arctan\left(\frac{I_5(i,j)-I_3(i,j)}{(I_1(i,j)+I_4(i,j))-(I_3(i,j)+I_5(i,j))}\right),$$
$$i=1,2,3, \tag{3}$$

where $\phi_i(x, y)$ belongs to $[-\pi, +\pi]$.

The absolute phase Φ_3 of λ_3 can be calculated by

$$\Phi_3(x,y)=\phi_3(x,y)+2\pi\left(\mathrm{INT}\left(\frac{\phi_{123}(x,y)}{2\pi}\times\frac{\lambda_{123}}{\lambda_{23}}\right)\times\frac{\lambda_{23}}{\lambda_3}+\mathrm{INT}\left(\frac{\phi_{23}(x,y)}{2\pi}\times\frac{\lambda_{23}}{\lambda_3}\right)\right). \tag{4}$$

When $\phi_3(x, y)$=2π, phase jump will occur, and Φ_3 is corrected as

$$\Phi_3'(x,y)=\begin{cases}\phi_3'(x,y)+2\pi\left(\mathrm{INT}\left(\frac{\phi_1'(x,y)}{2\pi}\times\frac{\lambda_1'}{\lambda_2'}\right)\times\frac{\lambda_2'}{\lambda_3'}+\mathrm{INT}\left(\frac{\phi_2'(x,y)}{2\pi}\times\frac{\lambda_2'}{\lambda_3'}\right)\right), & \phi_1'(x,y)\neq 2\pi \text{ and } \phi_2'(x,y)\neq 2\pi \text{ and } \phi_3'(x,y)\neq 2\pi.\\ \phi_3'(x,y)+2\pi\left(\mathrm{INT}\left(\frac{\phi_1'(x,y)}{2\pi}\times\frac{\lambda_1'}{\lambda_2'}\right)\times\frac{\lambda_2'}{\lambda_3'}+\mathrm{INT}\left(\frac{\phi_2'(x,y)}{2\pi}\times\frac{\lambda_2'}{\lambda_3}\right)-1\right), & \phi_1'(x,y)\neq 2\pi \text{ and } \left(\phi_2'(x,y)=2\pi \text{ or } \phi_3'(x,y)=2\pi\right).\\ \phi_3'(x,y)+2\pi\left(\mathrm{INT}\left(\frac{\phi_1'(x,y)}{2\pi}\times\frac{\lambda_1'}{\lambda_2'}-1\right)\times\frac{\lambda_2'}{\lambda_3'}+\mathrm{INT}\left(\frac{\phi_2'(x,y)}{2\pi}\times\frac{\lambda_2'}{\lambda_3'}\right)\right), & \phi_1'(x,y)=2\pi \text{ and } \phi_2'(x,y)\neq 2\pi \text{ and } \phi_3'(x,y)\neq 2\pi.\end{cases} \tag{5}$$

The main workflow of defect detection is shown as Fig.1. The first is to preprocess the data, including filtering and downsampling. The registration part is to extract the fast point feature histograms (FPFH) of the point cloud, use the SAC-IA algorithm for coarse registration, and then use the iterative closest point (ICP) algorithm for fine registration to determine whether there are defects based on the registration results[9,10]. Finally, the K-means clustering algorithm is used to cluster the pins and extract the parameter matrix of each pin region. The decision tree classifier is used to classify the defects.

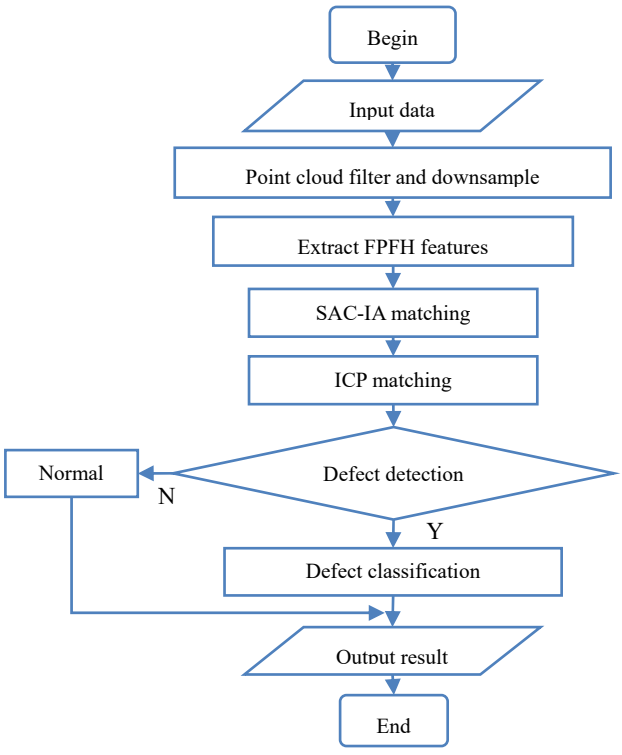

Fig.1 Process of the defect detection

Due to the influence of various artificial or random factors in the actual measurement process, irrational noise points will inevitably be mixed in the actual data. This paper uses a statistical-based filtering algorithm to filter the noisy data in the data. To be able to process data quickly and find defects, the original data must also be simplified. Therefore, under the premise of ensuring subsequent registration accuracy, the point cloud data is down-sampled.

Point cloud data registration can be divided into two parts: initial registration and precise registration. Different registration algorithms have different registration effects. In this paper, SAC-IA algorithm is used for initial registration and ICP method is used for accurate registration, so as to accurately locate the defect area.

The SAC-IA algorithm relies on point feature histograms (PFH). In order to improve the calculation speed, this paper calculates the FPFH of point cloud data. FPFH uses the estimated point cloud normal features to calculate the spatial difference between this point and its K domain points. After the data features are extracted, the next step is to match the data to be detected with the template data to obtain a rigid transformation matrix.

After using the SAC-IA algorithm for registration, the two point clusters roughly coincide, but there is still a deviation. In order to improve the matching accuracy between the two point clouds, it is necessary to perform accurate registration. The ICP algorithm is a widely used algorithm for fine registration and has a good convergence effect. The core goal of the ICP algorithm is to find the point with the smallest Euclidean distance in Q and P to obtain the transformation matrix. The minimized objective function can be obtained by

$$f(\boldsymbol{R},\boldsymbol{T}) = \arg\min \frac{1}{k}\sum_{i=1}^{k}\left\|q_i - (\boldsymbol{R}p_i + \boldsymbol{T})\right\|^2, \quad (6)$$

where $\boldsymbol{R}$ is the rotation matrix and $\boldsymbol{T}$ is the translation matrix, using the obtained transformation matrix to transform the target point cloud.

After registering the point cloud to be detected with the standard point cloud, the mean Euclidean distance (*MED*) deviation between the two point cloud data is calculated. That is, for each point p in P, the distanced of that point to the nearest point in Q is calculated. The *MED* can be obtained by

$$MED = \frac{\sum_{i=1}^{n}\sqrt{(x_i - x_{\text{nearst}})^2 + (y_i - y_{\text{nearst}})^2 + (z_i - z_{\text{nearest}})^2}}{n}, \quad (7)$$

where n is the number of point cloud.

It can be determined whether the current connector to be tested is defective. If there are defects, the K-means clustering algorithm is used to segment the connector pin data, and the minimum circumscribed rectangle and center of the defect area of each pin are calculated, as well as the average height of the pins in the region relative to the reference plane and data such as curvature and number of point clouds.

Usually, a missing pin defect is an empty location where the pin should exist. Therefore, the missing pin defects can be distinguished by judging the number of point clouds divided at this position. It is difficult to judge the curved needle defect and broken needle defect. Among these two types of defects, the broken needle has a noticeable height drop, and the number of point clouds is similar to the normal point cloud. In the case of curved pin, in the case of vertical scanning, the measurement area is large, so the number of point clouds is large, and the curvature of the point cloud data is very different from the standard data. It can be known that different judgment conditions are not continuous. Based on these judgments, a decision tree (DT) is used to classify the defects, and its structure is shown in Fig.2[11].

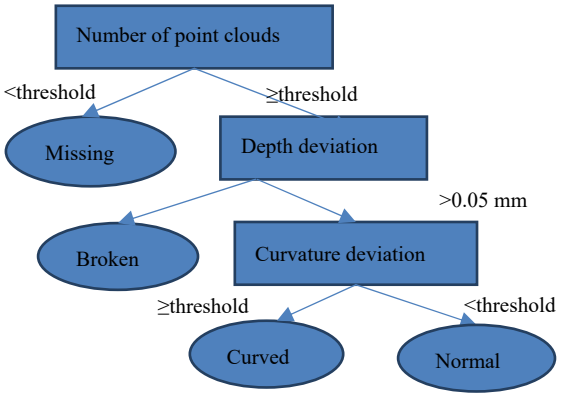

Fig.2 Decision tree composition

Fig.3 is the overall design structure of a 3D structured light measurement system. Among them, a type III independent optical projector with a resolution of 1 280×720 is used to project a sinusoidal stripe pattern with three different wavelengths. The three sinusoidal light periods are 1 008 pixels, 144 pixels and 16 pixels, respectively. Two industrial cameras (MV-CE050-30GM) send a 2 592×1 944 grayscale image to a computer at a frame rate of 14 frames per second. The angle of the two industrial cameras is 60°. Industrial cameras use a 16 mm (M1614-MP) lens. The model diagram of the main equipment is shown in Fig.3. When measuring connector data, the system is about 20 mm away from the measured object. The measurement range of this system is about 200 mm.

In order to further verify the accuracy of the 3D measurement system used in this paper, we adopted the traditional phase unwrapping method and the method proposed in this paper to project a calibration ball with a diameter of 20 mm. And use Geomagic studio to calculate the deviation between the radius of the fitted sphere and the standard sphere and the root mean square (*RMS*) error of the distance from each point to the fitted sphere. The comparison graph is shown in Fig.4 and the comparison results are shown in Tab.1. As shown in Tab.1, the radius error of the calibration sphere and the *RMS*

error of the sphere fitting obtained using the improved method are 0.008 3 mm and 0.016 1 mm, respectively. The TWPSP method is superior to traditional methods in radius error and *RMS* error, which fully proves the superiority of this method.

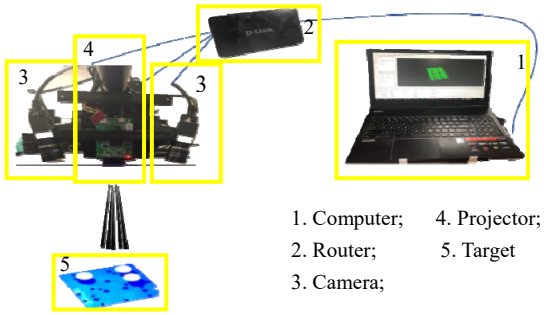

Fig.3 The 3D structured light measurement system

In order to further verify the accuracy of the 3D measurement system used in this paper, we adopted the traditional phase unwrapping method and the method proposed in this paper to project a calibration ball with a diameter of 20 mm. And use Geomagic studio to calculate the deviation between the radius of the fitted sphere and the standard sphere and the root mean square (*RMS*) error of the distance from each point to the fitted sphere. The comparison graph is shown in Fig.4 and the comparison results are shown in Tab.1. As shown in Tab.1, the radius error of the calibration sphere and the *RMS* error of the sphere fitting obtained using the improved method are 0.008 3 mm and 0.016 1 mm, respectively. The TWPSP method is superior to traditional methods in radius error and *RMS* error, which fully proves the superiority of this method.

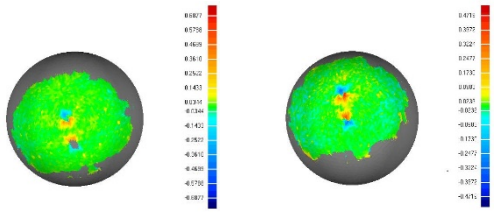

(a) The traditional method (b) The TWPSP method

Fig.4 Geomagic studio sphere fitting comparison

Tab.1 Data comparison of fitting results

Method	Radius error (mm)	*RMS* (mm)
The traditional method	0.013 7	0.031 4
The TWPSP method	0.008 3	0.016 1

The connector shown in Fig.5 is used as an experimental sample to verify the detection method mentioned in this article. The specific parameters of the experimental sample are as follows: the height of the plastic body is 8.5 mm, the length of the pins is 3.00 mm, there are a total of 16 pins, and the distance between adjacent pins is 2.54 mm.

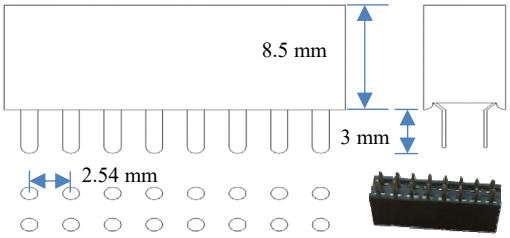

Fig.5 Parametric model of the connector

In order to verify the effectiveness of the registration algorithm, three registration algorithms were compared, including ICP algorithm based on FPFH features, ICP algorithm based on PFH features, and a combination of normal distribution transform (NDT) and ICP registration methods[12]. The registration results are shown in Tab.2. Among them, the NDT+ICP method takes the shortest time, but has the lowest registration accuracy. Both the FPFH+ICP and PFH+ICP methods have a rotating mean absolute error (*MAE*) of 0.002 4. The registration times of FPFH+ICP and PFH+ICP are 1.984 s and 3.525 s, respectively. It can be seen that with similar errors, the time consuming of FPFH+ICP is shorter. The data show that the performance of FPFH+ICP is better than the other two methods.

Tab.2 Comparison of different registration methods

	PFH+ICP	NDT+ICP	FPFH+ICP
X axis rotate error (mm)	0.002 8	0.005 1	0.004 3
Y axis rotate error (mm)	0.004 2	0.006 8	0.001 5
Z axis rotate error (mm)	-0.000 3	0.000 1	0.001 3
Rotating *MAE* (mm)	0.002 4	0.004 0	0.002 4
X axis translation error (mm)	0.000 1	0.000 1	0.000 1
Y axis translation error (mm)	0.000 1	0.000 3	0.000 2
Z axis translation error (mm)	-0.000 1	-0.000 3	-0.000 3
Translation *MAE* (mm)	0.000 1	0.000 26	0.000 2
Coarse registration time (s)	3.401	0.361	1.891
Fine registration time (s)	0.125	0.191	0.093
Total registration time (s)	3.525	0.544	1.984

The registration results are shown in Tab.3. It can be seen from Tab.3 that the *MED* between the defective connector and the standard connector is higher than 0.1 mm. It can be preliminarily judged that the connector to be tested has defects. The *MED* of non-destructive and standard connectors is less than 0.1 mm. As shown in Fig.6, Fig.6(a) is a defective point cloud, and Fig.6(c) is a non-defective point cloud. The registration results obtained by registering these two point clouds with the standard point cloud are shown in the Fig.6(b) and Fig.6(d). It can be seen that there are large differences in the registration results of defective point clouds, which verifies the calculation results of *MED*. The effectiveness

of this method is proved.

Tab.3 Comparison of registration results

	Defective connector	Nondestructive connector
MED (mm)	0.75	0.01

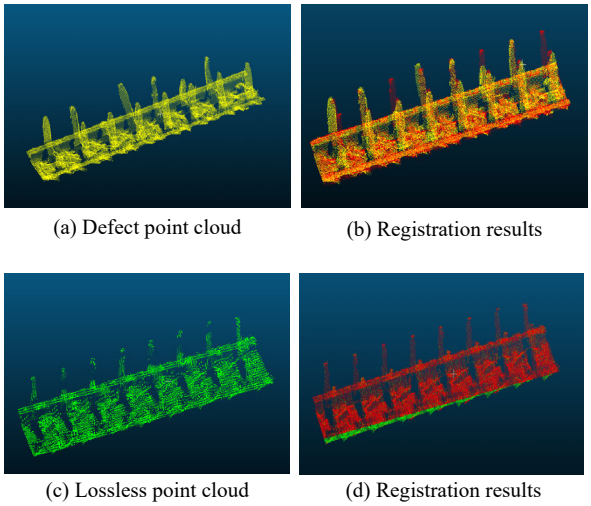

(a) Defect point cloud (b) Registration results

(c) Lossless point cloud (d) Registration results

Fig.6 Registration results

On this basis, in order to further verify the accuracy of the system's classification of connector defects, this article collected 50 double-row female connectors (60 bent pins, 30 broken pins, 10 fewer pins) with different defects as data.set. Pin defects are extracted from the cloud on the surface of the connector and are divided into three categories: missing pins, broken pins, and curved pins. The final classification results are shown in Tab.4.

Tab.4 Classification results of pin defect

Defect type		Predicted			
		Missing	Broken	Curved	Total
Actual	Missing	10	0	0	10
	Broken	2	28	0	30
	Curved	1	3	56	60
	Total	13	31	56	100

It can be seen from Tab.4 that the confusion matrix of the classification results obtained using the defect detection system constructed in this paper. The confusion matrix is used to evaluate the accuracy and reliability of the classification. A total of 97 defects were correctly classified, which indicates that the overall classification accuracy is 94%. The classification accuracy of fewer needles is 100% because fewer needle defects have more obvious characteristics. The number of point clouds and the average height in this area have a larger deviation than the tolerance matrix, which makes it easier to distinguish. However, there is a certain error between the broken needle defect and the curved needle defect because the parameters of the curved needle and broken needle defects are relatively similar, and it is more difficult to set the deviation threshold. Overall, the experimental results show that the classification method proposed in this paper is effective and reliable.

This paper uses a binocular structured light 3D measurement system to accurately and efficiently obtain the point cloud data of the connector. An improved phase expansion algorithm is also proposed. The improved phase expansion algorithm can effectively avoid error propagation in the phase superposition process. On the other hand, the FPFH+ICP algorithm is used to achieve sub-millimeter registration accuracy, which makes it possible to quickly determine defects. In addition, the K-means algorithm is used to perform cluster segmentation on the defective pins. For each area, a decision tree classifier is used to identify the defect type of the pin. The experimental results show that the proposed detection algorithm can register the surface profile of the connector with the standard connector data, determine whether there is a defect, and achieve good performance in defect classification. In future work, we will try other machine learning algorithms, such as SVM, to train the classifier to further improve the accuracy of classification.

References

[1] Chen S H and Perng D B, Journal of Intelligent Manufacturing **27**, 915 (2016).

[2] Kuo C F J, Hsu C T M and Liu Z X, Journal of Intelligent Manufacturing **25**, 1235 (2014).

[3] Adaškevičius R and Vasiliauskas A, Electronics and Electrical Engineering **82**, 49 (2015).

[4] Gao Yan, Shao Shuangyun and Feng Qibo, Chinese Journal of Lasers **40**, 182 (2013).

[5] J. Geng, Advances in Optics and Photonics **3**, 128 (2011).

[6] Lee M C, Chen W T and Lin C T, Microsystems, Packaging, Assembly and Circuits Technology Conference **11**, 145 (2012).

[7] Wei Z, Xiao Z and Zhang X, Proceedings of SPIE - The International Society for Optical Engineering **12**, 76 (2011).

[8] Limei Song, Yulan Chang, Jiangtao Xi, Qinghua Guo, Xinjun Zhu and Xiaojie Li, Optics Communications **35**, 213 (2015).

[9] Lu Jun, Peng Zhongtao and Dong Donglai, New Industrialization **7**, 75 (2014).

[10] Yang Cong, Dongying Tian and Yun Feng, IEEE Transactions on Cybernetics **99**, 1 (2018).

[11] Katherine E. Goodman, Justin Lessler and Sara E, Clinical Infectious Diseases **7**, 63 (2016).

[12] Todor Stoyanov, Martin Magnusson and Hakan Almqvist, IEEE International Conference on Robotics and Automation, 2011.